photonics

MDPI

Article

Optical and Scintillation Properties of Tb-Doped Rare-Earth Pyrosilicate Single Crystals

Prom Kantuptim [1], Takumi Kato [1], Daisuke Nakauchi [1], Noriaki Kawaguchi [1], Kenichi Watanabe [2] and Takayuki Yanagida [1,*]

[1] Division of Materials Science, Graduate School of Science and Technology, Nara Institute of Science and Technology, 8916-5 Takayama, Nara 630-0192, Japan
[2] Department of Applied Quantum Physics and Nuclear Engineering, Faculty of Engineering, Kyushu University, 744 Motooka, Fukuoka 819-0395, Japan
* Correspondence: t-yanagida@ms.naist.jp

Abstract: Series of 1.0% Terbium (Tb)-doped rare-earth pyrosilicate single crystals including $Lu_2Si_2O_7$ (LPS), $Y_2Si_2O_7$ (YPS), $Gd_2Si_2O_7$ (GPS), and $La_2Si_2O_7$ (LaPS) have been prepared by the floating-zone method. After the phase confirmation by powder X-ray diffraction, the properties are measured on both photoluminescence and scintillation aspects, including the photoluminescence emission contour graph and decay times, X-ray induced scintillation spectra and decay times, afterglow profiles, and the recently developed pulse height spectra for scintillators with millisecond decay time. The results indicate the multiple emissions from Tb^{3+} 4f-4f transition with the dominant emission at 540 nm ($^5D_4 \rightarrow {}^7F_5$) on both ultraviolet and X-ray excitation with the decay time around 2.6–5.6 and 1.3–3.2 ms, respectively. Under the γ-ray irradiation from ^{137}Cs, the Tb-doped LPS, YPS, GPS, and LaPS have presented scintillation light yields of 20,700, 29,600, 95,600, and 47,700 ph/MeV with ±10%, respectively, which considerably very high among the oxide scintillators.

Keywords: scintillator 1; Tb^{3+} 2; pulse-height 3

Citation: Kantuptim, P.; Kato, T.; Nakauchi, D.; Kawaguchi, N.; Watanabe, K.; Yanagida, T. Optical and Scintillation Properties of Tb-Doped Rare-Earth Pyrosilicate Single Crystals. *Photonics* **2022**, *9*, 765. https://doi.org/10.3390/photonics9100765

Received: 1 September 2022
Accepted: 11 October 2022
Published: 13 October 2022

1. Introduction

A scintillator is a special category in luminescence materials that have the ability to convert the ionizing radiation and charge particles to lower energy photons such as ultraviolet, visible, and infrared light [1,2]. From this unique property, a combination between scintillator materials and the photodetector or so-called scintillation detector has been implemented in many professional fields related to ionizing radiation including medical [3,4], astrophysics [5,6], geophysics [7–10], environmental observation [11–14], homeland security [15–18], natural resource exploration [19,20], and more. For each application with different demands, scintillator materials have come in various forms of materials such as single crystal [21–26], polymer [27–31], glass [32–36], transparent ceramics [37–41], and inorganic-organic perovskite composite [42–45]. In the present day, the lanthanide-doped single crystal is one of the main focus materials for the scintillator in both academic and industrial fields because of attractive scintillation properties [46]. Pyrosilicate materials are one of the interesting host materials for lanthanide doped oxide single crystal scintillator. One of the examples and the earliest report of pyrosilicate scintillator is Ce-doped $Lu_2Si_2O_7$ (LPS) with impressive scintillation properties such as high light yield at 26,300 ph/MeV and fast decay time of 38 ns [47–52]. Since the introduction of the Ce-doped LPS, the research of the pyrosilicate crystal has become popular for the novel oxide scintillators through changing the rare-earth ions in the host and luminescence center to other rare earth ions, and examples are Ce-doped $Y_2Si_2O_7$ (YPS) [53] and Nd-doped LPS [54]. However, in the past, the evaluation of scintillation light yield which was measured by conventional pulse height measurement was limited to the scintillators with a decay time of less than milliseconds. Until recently, the Tb-doped $Sr_2Gd_8(SiO_4)_6O_2$ has been the first report on ms

decay time scintillator with scintillation light yield measured by a newly developed system [55]. The combination between the ms decay time luminescence center such as Tb and the pyrosilicate crystal has not been studied, and Tb-doped pyrosilicate is expected to have high light yield.

This study is the first investigation to introduce Tb to the various pyrosilicate single crystals including LPS, YPS, $Gd_2Si_2O_7$ (GPS), and $La_2Si_2O_7$ (LaPS). The characterizations of these compounds are focused on both photoluminescence (PL) and scintillation properties including PL emission, PL decay time, scintillation spectrum, scintillation decay time, afterglow level, and newly developed pulse height spectra for ms decay time scintillator. In addition, this report also provides the possibility, trends, and potentials of combination between Tb as luminescence center in the different rare-earth pyrosilicate.

2. Materials and Methods

The Tb-doped LPS, YPS, GPS, and LaPS samples are carefully synthesized by following orders. First, the 99.99% purity powder of raw materials in including SiO_2, Tb_4O_7, Lu_2O_3 (for LPS), Y_2O_3 (for YPS), Gd_2O_3 (for GPS), and Lu_2O_3 (for LaPS) has been weighted and mixed by an agate mortar. Tb concentration in every sample is fixed to the 1.0 mol% with respect to each rare-earth site (Lu, Y, Gd, and La). The well-mixed powder has been shaped to the rod by applying isostatic pressure. Each obtained rod is sintering in the furnace for 10 h at 1200 °C for LPS, YPS, and GPS, and 1400 °C for LaPS. By these sintered ceramic rods, single crystal growth is done by desktop floating-zone furnace (FZD0192, Canon machinery). The furnace uses two halogen lamps as a heat source. The crystal growth rate is 4 mm/h. The obtained single crystal rods are cut to 1 mm in thickness and polished on both sides of the surface. The leftover crystals pieces from the cutting process have been ground for phase confirmation by powder X-ray diffraction (MiniFlex600, Rigaku Corporation, Tokyo, Japan). The polished samples have been used for diffused transmittance measurement by spectrophotometer (SolidSpec-3700, Shimadzu Corporation, Kyoto, Japan) at a wavelength of 200–800 nm. The PL emission contour graph and PL quantum yield (*QY*) are achieved by using Quantaurus-QY (C11347-01, Hamamatsu Photonics K.K., Shizuoka, Japan), with excitation wavelength from 250–400 nm and observation wavelength from 300–700 nm. On the other hand, The PL decay time analysis is performed by Quantaurus-τ (C11367, Hamamatsu Photonics K.K., Shizuoka, Japan). The excitation light is controlled by a halogen lamp with the applied 340–390 nm bandpass filter. The observation wavelength is 550 nm which is generated from Tb^{3+} 4f-4f emission.

In the scintillation properties, X-ray induced scintillation spectra are performed by our original setup [56]. The irradiated X-ray dose used for spectrum observation is 1 Gy. X-ray induced scintillation decay time and the afterglow analysis are also performed by using our original system equipped with the pulsed X-rays source and the afterglow characterization system [57]. The observation wavelength is from 160–650 nm. The calculation of the afterglow level is consistent with our previous works as the following equation [58,59], $Af_{20} = (I_{20}\text{-}I_{bg})/I_{max}$ when the Af_{20} is the afterglow level at 20 ms after X-ray irradiation, I_{20} is the signal intensity at 20 ms after X-ray irradiation, I_{bg} is the signal intensity before X-ray irradiation or so call background intensity, and I_{max} is the maximum value of the signal intensity during the X-ray irradiation. The pulse height spectra and absolute scintillation light yield of the Tb-doped pyrosilicate samples are measured by the recently developed ms decay time pulse height setup [55]. Strictly speaking, the spectrum observed by this setup is not a pulse height but a pulse area. However, the physical meaning is the same, and to avoid complexity, the common term of pulse height is used in this work. In this measurement, the voltage of −550 V has been applied to the PMT (R7600U-200, Hamamatsu Photonics), thus the signal from PMT is sent to the digitizer (Model 1819-16, Clear Pulse). ^{137}Cs has been selected for a γ-ray source (662 keV). In addition, a $Bi_4Ge_3O_{12}$ (BGO) scintillator with a scintillation light yield of 8200 ph/MeV has been selected as a reference sample for this measurement [60].

3. Results and Discussions

3.1. Sample Conditions

Figure 1a presents the photographs of Tb-doped LPS, YPS, GPS, and LaPS single crystal rods obtained from the floating-zone method, with the crystal rods length of 20–25 mm and diameter of 4 mm. The visible cracks throughout the entire crystal rods appear in every sample. The cracks are consistent with the previous attempt on the crystal growth of pyrosilicate crystals by the floating zone method [61,62]. However, after cut and polished, relatively clear and transparent sample is obtained as presented in Figure 1b, with the bright yellow-green luminescence from the Tb-doped under the 254 nm UV lamp presented in Figure 1a. Figure 2 shows the XRD patterns of the Tb-doped LPS, YPS, GPS, and LaPS powders with an individual reference pattern. Similar to our previous reports, the Tb-doped LPS and YPS patterns belong to monoclinic $Lu_2Si_2O_7$ (COD 8400597) [63] and $Y_2Si_2O_7$ (JCPDS 82-0732) [64], respectively. The Tb-doped GPS pattern agrees with orthorhombic $Gd_2Si_2O_7$ (COD 9011106) [65], and that of Tb-doped LaPS pattern matches with monoclinic $Lu_2Si_2O_7$ (JCPDS 82-0729) [66]. In all four samples, no impurity phases are detected. In addition, the substitution of 1 mol% Tb to rare-earth site in the pyrosilicate structure is achieved and not affected the XRD pattern.

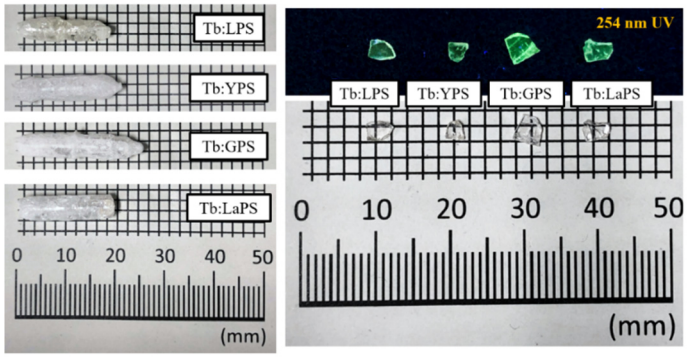

(**a**) (**b**)

Figure 1. Tb-doped LPS, YPS, GPS, and LaPS samples photographs of (**a**) as-grown single crystal rods; (**b**) cut and polished specimens in room light and 254 nm UV.

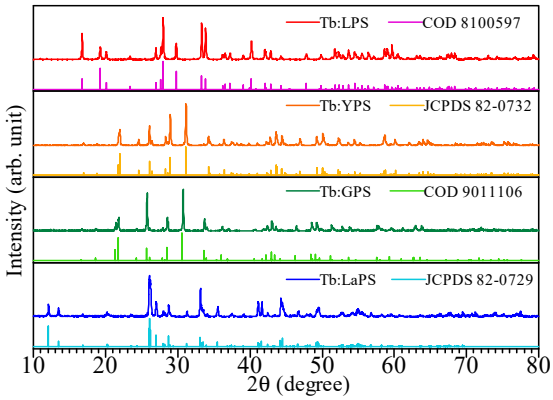

Figure 2. XRD pattern of Tb-doped LPS, YPS, GPS, and LaPS samples, with each individual reference pattern.

Figure 3 shows the diffuse transmittance spectra of the Tb-doped LPS, YPS, GPS, and LaPS sample. From 400 to 800 all the samples have transmittance over 80% which indicated good transparency of the polished samples presented in Figure 1b. The absorption band of the Tb^{3+} 4f-4f is start from 240–350 nm. However, the Tb-doped GPS sample have more complicated shape of the absorption band than the other Tb-doped pyrosilicate in this

study. The explanation of this behavior is discussed with the additional results from the later PL property.

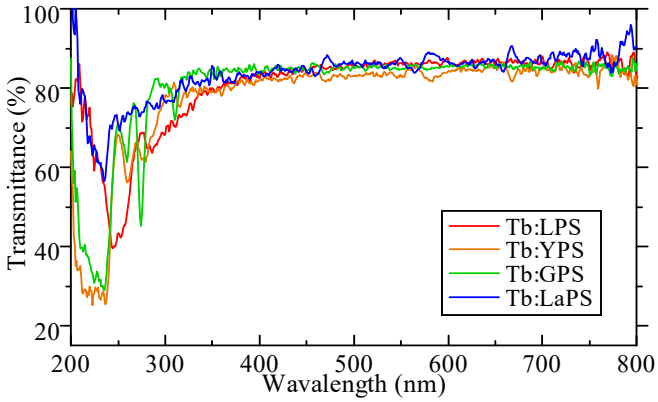

Figure 3. Diffused transmittance spectra of Tb-doped LPS, YPS, GPS, and LaPS samples.

3.2. Photoluminescence Propterties

Figure 4 presents the PL excitation and emission contour graph of Tb-doped pyrosilicate samples with excitation and emission ranges of 250–400 and 300–700 nm, respectively. All the samples have presented a similar emission characteristic of Tb^{3+} 4f-4f transitions. The detail of each emission will discuss in the next result of scintillation spectra. The highest emission intensity of all the samples is 540 nm due to $^5D_4 \rightarrow {}^7F_5$ transition of Tb^{3+}. Despite the similarity in emission wavelength, the excitation characteristic of Tb-doped GPS is different from the rest of Tb-doped pyrosilicate counterparts. The main excitation wavelength of Tb-doped GPS is shifted from 270 nm in the other samples to 310 nm with a significantly higher *QY* at 68.9% than the Tb-doped LPS, YPS, and LaPS at 29.7, 13.6, and 21.6%, respectively. The possible reasons for the shifting of major excitation in Tb-doped GPS are effected by the intrinsic emission of GPS at 310 nm by Gd^{3+} 4f-4f transition which observed in the study of undoped GPS crystal [67].

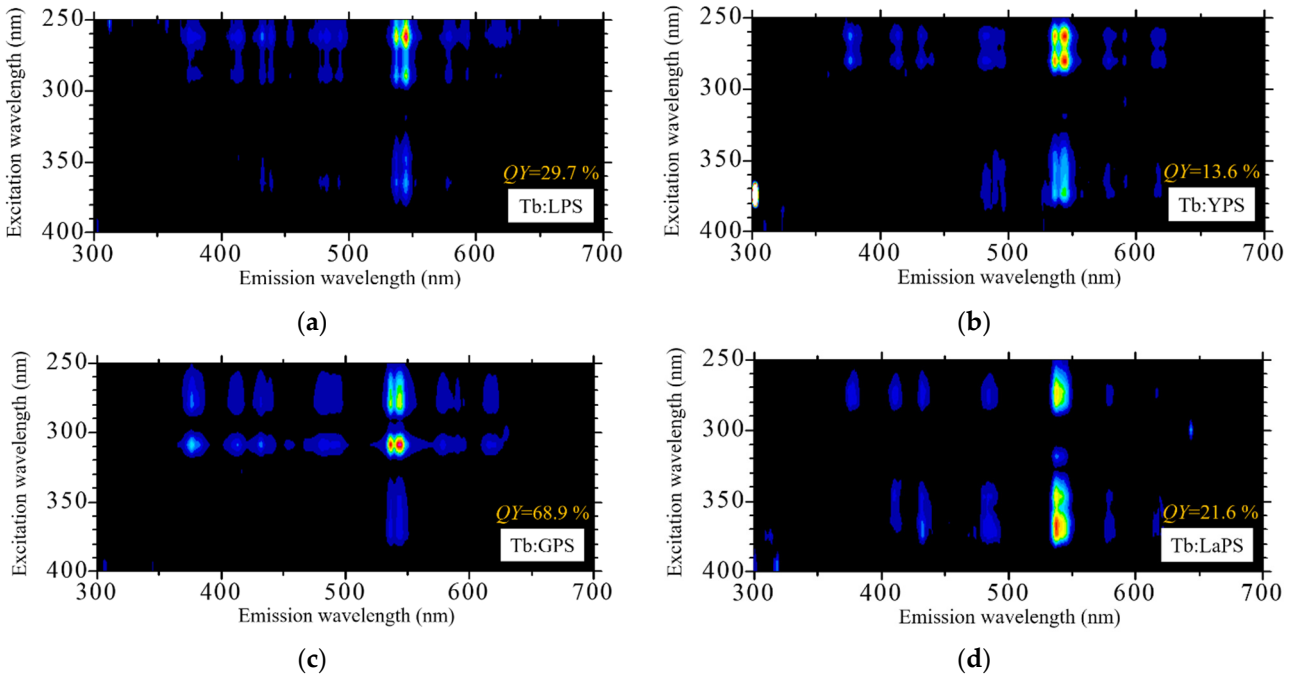

Figure 4. PL excitation and emission contour graph of (**a**) Tb-doped LPS; (**b**) Tb-doped YPS; (**c**) Tb-doped GPS; (**d**) Tb-doped LaPS.

Figure 5 exhibits the PL decay time profiles of each Tb-doped LPS, YPS, GPS, and LaPS sample. In the initial part of the profile, every sample in this study presents a slow rise in the signal intensity. This part of the profile is possibly influenced by the instrumental response function which is represented by cyan lines in all the four sample profiles. The fitting is done by excluding the influenced part by the IRF, and fitting results by a single exponential function is also as presented in Figure 4 below the name of each sample. The PL decay times of Tb-doped LPS, YPS, GPS, and LaPS samples are 2.62, 5.65, 5.29, and 3.04 ms, respectively. The results are consistent with the previous study on Tb-doped scintillator materials [68].

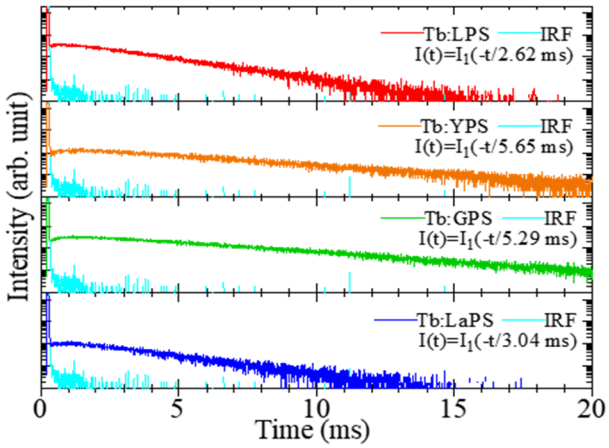

Figure 5. PL decay time profiles of Tb-doped LPS, YPS, GPS, and LaPS samples. Observation and excitation wavelength are 550 and 340–390 nm, respectively.

3.3. Scintillation Properties

Figure 6 presents X-ray induced scintillation spectra of Tb-doped LPS, YPS, GPS, and LaPS samples. All of the samples have the same spectral shape. Furthermore, the scintillation wavelengths observed here are similar to the emission wavelength with the results of PL emission. In addition, the scintillation from Tb^{3+} 4f-4f transitions including 380 ($^5D_3 \rightarrow {}^7F_6$), 420 ($^5D_3 \rightarrow {}^7F_5$), 440 ($^5D_4 \rightarrow {}^7F_5$), 480 ($^5D_4 \rightarrow {}^7F_6$), 540 ($^5D_4 \rightarrow {}^7F_5$, strongest), 590 ($^5D_4 \rightarrow {}^7F_4$), and 620 nm ($^5D_4 \rightarrow {}^7F_3$) are founded in all sample. In terms of spectral shapes, the scintillation spectra of Tb-doped pyrosilicate samples are comparable to the other Tb-doped scintillator study. Because the intensity value (vertical axis) in this measurement is qualitative, the comparison of scintillation light yield is discussed in the pulse-height spectra results.

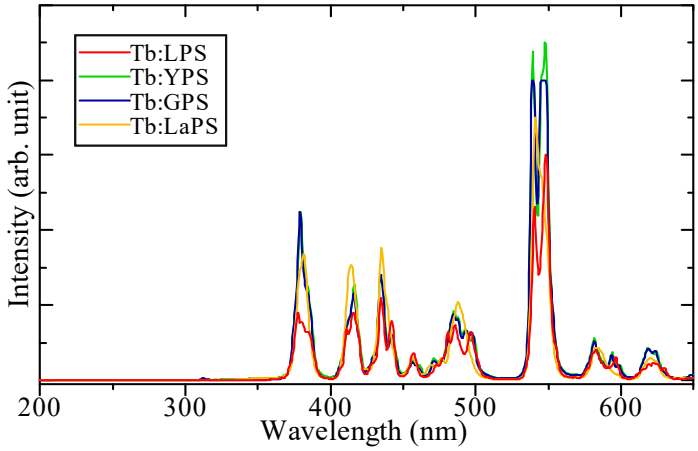

Figure 6. X-ray induced scintillation spectra of Tb-doped LPS, YPS, GPS, and LaPS samples.

Figure 7 illustrates the X-ray induced scintillation decay time profile of each Tb-doped LPS, YPS, GPS, and LaPS sample. The decay time profile is approximated with a sum of two exponential decay functions. The 1st decay constant of all samples is influenced by the IRF which appears at the initial part of the profile as a very fast component. On the other hand, the 2nd decay constant of the samples is ascribed to the scintillation from the Tb^{3+} 4f-4f transitions. When comparing with the previous results of PL decay times, every sample has shown a faster scintillation decay constant [69]. This phenomenon may be caused by the wavelength sensitivity of this measurement from 160 to 650 nm. In PL, only the emission at 540 nm is focused by using optical filters while the current measurements accumulate all the emissions from 160 to 650 nm. The afterglow timing profiles of Tb-doped LPS, YPS, GPS, and LaPS samples and Af_{20} values are exhibited in Figure 8. In comparison with the commercial scintillator on the market, Tb-doped pyrosilicate samples have relatively higher afterglow levels than the $CdWO_4$ (CWO) and Tl-doped CsI which have Af_{20} around 100 and 268 ppm, respectively [70,71]. One of the main reasons for the Tb-doped pyrosilicate sample's high afterglow level is the slow scintillation decay time in the ms region.

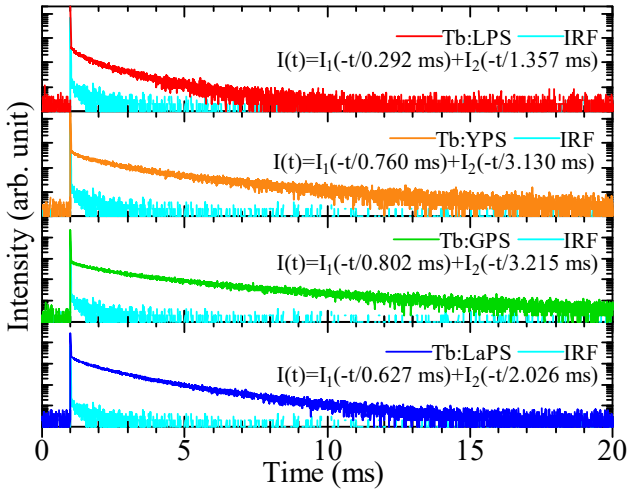

Figure 7. X-ray induced scintillation decay time of Tb-doped LPS, YPS, GPS, and LaPS samples.

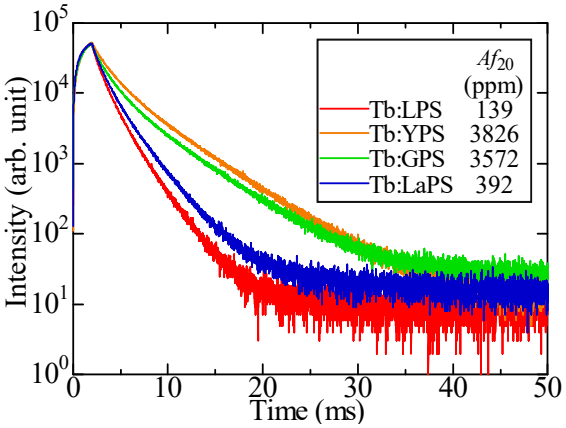

Figure 8. Afterglow profiles of Tb-doped LPS, YPS, GPS, and LaPS samples, with the Af_{20}.

Figure 9 presents the pulse-height spectra of Tb-doped pyrosilicate samples, under the ^{137}Cs (662 keV) γ-ray irradiation, plotted with the spectrum of the BGO reference sample. For the scintillation light yield, the calculation is done by taking into consideration the different quantum efficiencies of the PMT on both scintillation wavelengths of Tb-doped pyrosilicate (540 nm, 9%) and BGO reference (480 nm, 25%). It means, although photoabsorption peak channels of Tb-doped YPS and reference BGO are close, after the

correction of quantum efficiency of PMT, Tb-doped YPS sample will have the scintillation light yield 2.77 time higher than the BGO reference. The calculated scintillation light yield with an energy resolution of each sample and BGO reference are summarized in Table 1. Among all of the Tb-doped pyrosilicate samples in this study, the Tb-doped GPS has presented the highest scintillation light yield of 95,600 ph/MeV. The combination of the Gd site in the host and the Tb^{3+} ions as luminescence center is one of the possible reasons why Tb-doped GPS has higher scintillation light yield than the other sample. According to PL emission map (Figure 3), only Tb-doped GPS shows the excitation wavelength of 310 nm unlike other samples having that of 270 nm. In our previous work of undoped GPS, it showed an emission peak at 310 nm [67]. In Tb-doped GPS, the emitted photons of 310 nm from the host has been self-absorbed and then transferred to emission by $^5D_4 \rightarrow {}^7F_5$ transitions of Tb^{3+} at 540 nm. however, the energy resolution is 30.3% considerably high and not favorable for a scintillator. On the other hand, Tb-doped LaPS is also interesting due to its better energy resolution of 16.8% and still had high scintillation light yield of 47,700 ph/MeV. For the next step, the improvement of the crystal quality is recommended in future work such as changing the crystal growth method to a more delicate way such as Czochralski-method to improve the energy resolution and the other properties.

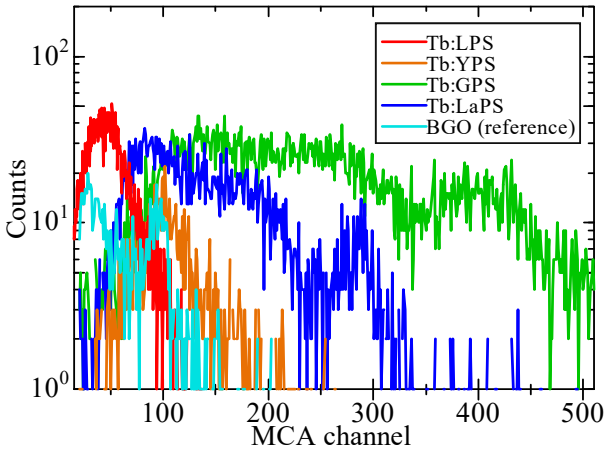

Figure 9. Pulse-height spectra of Tb-doped LPS, YPS, GPS, and LaPS samples, under the ^{137}Cs (662 keV) γ-ray. With the spectrum of the BGO reference sample.

Table 1. Absolute scintillation light yields and energy resolution of the Tb-doped pyrosilicate samples under 662 keV γ-ray irradiation.

Sample Name	Scintillation Light Yield (ph/MeV)	Energy Resolution (%)
Tb-doped LPS	20,700	15.2
Tb-doped YPS	29,600	10.6
Tb-doped GPS	95,600	30.3
Tb-doped LaPS	47,700	16.8
BGO	8200 [60]	26.9

4. Conclusions

1.0% Tb-doped LPS, YPS, GPS, and LaPS single crystals are successfully grown by the floating-zone technique. The single phase of each rare-earth pyrosilicate is validated by powdered XRD analysis. PL properties of the samples are investigated including multiple emissions characterized by the strongest emission at 540 nm of Tb^{3+} 4f-4f transitions on PL emission contour graphs, and the PL decay times of the present samples are 2.62–5.65 ms. In scintillation properties, X-ray induced scintillation spectra of the samples have presented similar emission peaks with PL. The scintillation decay times of the samples resulted in 1.35–3.21 ms. The Tb-doped YPS and GPS present a high afterglow level (Af_{20}) at around 3500–3800 ppm. Under 662 keV γ-ray irradiation by ^{137}Cs, the Tb-doped

pyrosilicate samples present high scintillation light yield, and especially Tb-doped GPS shows 95,600 ph/MeV with the energy resolution of 30.3%. The Tb-doped LaPS exhibits the second highest scintillation light yield in this study with 47,700 ph/MeV with an energy resolution of 16.8%. To the presented results, Tb-doped GPS and LaPS are suitable candidates for the novel scintillator. However, Tb-doped pyrosilicate materials have scintillation decay time in the ms-range. Therefore, the possible applications are the ones that favor brightness over the response time such as the scintillator screen for X-ray radiography. In the future work of these materials, the Tb-doped concentration dependence and the other method of crystal growth are recommended for the Tb-doped GPS and LaPS for improving and better understanding properties of these compounds.

Author Contributions: Conceptualization, P.K.; methodology, P.K., K.W. and T.Y.; validation, T.K., D.N. and N.K.; formal analysis, P.K. and T.Y.; investigation, P.K., K.W. and T.Y.; resources, K.W. and T.Y.; data curation, P.K. and N.K.; writing—original draft preparation, P.K.; writing—review and editing, P.K.; visualization, P.K.; supervision, T.Y.; funding acquisition, T.K., D.N., N.K. and T.Y. All authors have read and agreed to the published version of the manuscript.

Funding: This work was supported by the Cooperative Research Project of the Research Center for Biomedical Engineering, Nippon Sheet Glass Foundation, and Iketani Science and Technology. In addition, the Japan Society for the Promotion of Science (JSPS) is also acknowledged for Grant-in-Aid for Scientific Research A (22H00309), B (21H03733, 21H03736, and 22H02939), Grant-in-Aid for Exploratory Research (22K18997), and Early-Career Scientists (20K20104).

Institutional Review Board Statement: Not applicable.

Informed Consent Statement: Not applicable.

Data Availability Statement: Data of the results presented in this article are not publicly available.

Acknowledgments: Radiation Physics and Measurement Laboratory, Department of Applied Quantum Physics and Nuclear Engineering, Faculty of Engineering, Kyushu University is acknowledged for providing the measurements system and data curations.

Conflicts of Interest: The authors declare no conflict of interest.

References

1. van Eijk, C.W.E. Inorganic-scintillator development. *Nucl. Instrum. Methods Phys. Res. B* **2001**, *460*, 1–14. [CrossRef]
2. Kumar, V.; Luo, Z. A review on x-ray excited emission decay dynamics in inorganic scintillator materials. *Photonics* **2021**, *8*, 71. [CrossRef]
3. Ronda, C.; Wieczorek, H.; Khanin, V.; Rodnyi, P. Review-scintillators for medical imaging: A tutorial overview. *ECS J. Solid State Sci. Technol.* **2016**, *5*, R3121–R3125. [CrossRef]
4. Arifuzzaman, M.; Ranasinghe, M.; Rajamanthrilage, A.C.; Bhattacharya, S.; Anker, J.N. Fast and Inexpensive Separation of Bright Phosphor Particles from Commercial Sources by Gravitational and Centrifugal Sedimentation for Deep Tissue X-ray Luminescence Imaging. *Photonics* **2022**, *9*, 347. [CrossRef]
5. Bloser, P.F.; Legere, J.S.; Bancroft, C.M.; McConnell, M.L.; Ryan, J.M. Scintillators with silicon photomultiplier readouts for high-energy astrophysics and heliophysics. In *Proceedings of the Space Telescopes and Instrumentation 2014: Ultraviolet to Gamma Ray, Montréal, Canada, 22–26 June 2014*; Takahashi, T., den Herder, J.-W.A., Bautz, M., Eds.; SPIE: Bellingham, WA, USA, 2014; Volume 9144, p. 914414.
6. Fuschino, F.; Campana, R.; Labanti, C.; Evangelista, Y.; Feroci, M.; Burderi, L.; Fiore, F.; Ambrosino, F.; Baldazzi, G.; Bellutti, P.; et al. HERMES: An ultra-wide band X and gamma-ray transient monitor on board a nano-satellite constellation. *Nucl. Instrum. Methods Phys. Res. B* **2019**, *936*, 199–203. [CrossRef]
7. Parshin, A.; Morozov, V.; Snegirev, N.; Valkova, E.; Shikalenko, F. Advantages of gamma-radiometric and spectrometric low-altitude geophysical surveys by unmanned aerial systems with small scintillation detectors. *Appl. Sci.* **2021**, *11*, 2247. [CrossRef]
8. Yuasa, T.; Wada, Y.; Enoto, T.; Furuta, Y.; Tsuchiya, H.; Hisadomi, S.; Tsuji, Y.; Okuda, K.; Matsumoto, T.; Nakazawa, K.; et al. Thundercloud Project: Exploring high-energy phenomena in thundercloud and lightning. *Prog. Theor. Exp. Phys.* **2020**, *2020*, 103H01. [CrossRef]
9. Enoto, T.; Wada, Y.; Furuta, Y.; Nakazawa, K.; Yuasa, T.; Okuda, K.; Makishima, K.; Sato, M.; Sato, Y.; Nakano, T.; et al. Photonuclear reactions triggered by lightning discharge. *Nature* **2017**, *551*, 481–484. [CrossRef] [PubMed]
10. Wada, Y.; Matsumoto, T.; Enoto, T.; Nakazawa, K.; Yuasa, T.; Furuta, Y.; Yonetoku, D.; Sawano, T.; Okada, G.; Nanto, H.; et al. Catalog of gamma-ray glows during four winter seasons in Japan. *Phys. Rev. Res.* **2021**, *3*, 7–9. [CrossRef]

11. Zou, Y.; Zhang, W.; Li, C.; Liu, Y.; Luo, H. Construction and test of a single sphere neutron spectrometer based on pairs of ^{6}Li-and ^{7}Li-glass scintillators. *Radiat. Meas.* **2019**, *127*, 106143. [CrossRef]
12. Lee, H.C.; Shin, W.G.; Choi, H.J.; Choi, C.I.; Park, C.S.; Kim, H.S.; Min, C.H. Radioisotope identification using an energy-weighted algorithm with a proof-of-principle radiation portal monitor based on plastic scintillators. *Appl. Radiat. Isot.* **2020**, *156*, 109010. [CrossRef] [PubMed]
13. Paff, M.G.; Di Fulvio, A.; Clarke, S.D.; Pozzi, S.A. Radionuclide identification algorithm for organic scintillator-based radiation portal monitor. *Nucl. Instrum. Methods Phys. Res. B* **2017**, *849*, 41–48. [CrossRef]
14. Ryzhikov, V.D.; Naydenov, S.V.; Piven, L.A.; Onyshchenko, G.M.; Smith, C.F.; Pochet, T. Fast neutron detectors and portal monitors based on solid-state heavy-oxide scintillators. *Radiat. Meas.* **2017**, *105*, 17–25. [CrossRef]
15. Cieślak, M.; Gamage, K.; Glover, R. Critical Review of Scintillating Crystals for Neutron Detection. *Crystals* **2019**, *9*, 480. [CrossRef]
16. Liu, Q.; Cheng, Y.; Yang, Y.; Peng, Y.; Li, H.; Xiong, Y.; Zhu, T. Image reconstruction using multi-energy system matrices with a scintillator-based gamma camera for nuclear security applications. *Appl. Radiat. Isot.* **2020**, *163*, 109217. [CrossRef] [PubMed]
17. Glodo, J.; Wang, Y.; Shawgo, R.; Brecher, C.; Hawrami, R.H.; Tower, J.; Shah, K.S. New Developments in Scintillators for Security Applications. *Phys. Procedia* **2017**, *90*, 285–290. [CrossRef]
18. Ryzhikov, V.D.; Opolonin, A.D.; Pashko, P.V.; Svishch, V.M.; Volkov, V.G.; Lysetskaya, E.K.; Kozin, D.N.; Smith, C. Instruments and detectors on the base of scintillator crystals ZnSe(Te), CWO, CsI(Tl) for systems of security and customs inspection systems. *Nucl. Instrum. Methods Phys. Res. B* **2005**, *537*, 424–430. [CrossRef]
19. Yanagida, T.; Fujimoto, Y.; Kurosawa, S.; Kamada, K.; Takahashi, H.; Fukazawa, Y.; Nikl, M.; Chani, V. Temperature dependence of scintillation properties of bright oxide scintillators for well-logging. *Jpn. J. Appl. Phys.* **2013**, *52*, 3–9. [CrossRef]
20. Melcher, C.L. Scintillators for well logging applications. *Nucl. Instrum. Methods Phys. Res. Sect. B Beam Interact. with Mater. Atoms* **1989**, *40–41*, 1214–1218. [CrossRef]
21. Fujimoto, Y.; Nakauchi, D.; Yanagida, T.; Koshimizu, M.; Asai, K. New Intrinsic Fast Scintillator: Cesium Praseodymium Chloride. *Sens. Mater.* **2022**, *34*, 629–636. [CrossRef]
22. Rinaldi, D.; Montalto, L.; Lebeau, M.; Mengucci, P. Influence of a surface finishing method on light collection behaviour of PWO scintillator crystals. *Photonics* **2018**, *5*, 47. [CrossRef]
23. Matsuoka, M.; Higuchi, M.; Nishikido, F.; Yamaya, T.; Takeda, T.; Masubuchi, Y.; Kaneko, J.H. Spectral properties and β-ray scintillation of $GdVO_4$:Eu single crystals grown by the floating zone method. *J. Lumin.* **2022**, *251*, 119208. [CrossRef]
24. Chaiphaksa, W.; Borisut, P.; Kim, H.J.; Kothan, S.; Kaewkhao, J. Photon interaction of molybdenum (Mo) based cesium trimolybdate ($Cs_2Mo_3O_{10}$) and disodium dimolybdate ($Na_2Mo_2O_7$) single crystal scintillators. *Radiat. Phys. Chem.* **2022**, *201*, 110373. [CrossRef]
25. Rutstrom, D.; Stand, L.; Delzer, C.; Kapusta, M.; Glodo, J.; van Loef, E.; Shah, K.; Koschan, M.; Melcher, C.L.; Zhuravleva, M. Improved light yield and growth of large-volume ultrafast single crystal scintillators Cs_2ZnCl_4 and Cs_3ZnCl_5. *Opt. Mater.* **2022**, *133*, 112912. [CrossRef]
26. Tariwong, Y.; Vuong, P.Q.; Luan, N.T.; Saha, S.; Kim, H.J.; Wantana, N.; Chanthima, N.; Kaewkhao, J.; Kothan, S. Crystal growth and scintillation properties of Tm^{3+} doped $LaCl_3$ single crystal for radiation detection. *Radiat. Phys. Chem.* **2022**, *200*, 110347. [CrossRef]
27. Zaitseva, N.; Rupert, B.L.; Pawełczak, I.; Glenn, A.; Martinez, H.P.; Carman, L.; Faust, M.; Cherepy, N.; Payne, S. Plastic scintillators with efficient neutron/gamma pulse shape discrimination. *Nucl. Instrum. Methods Phys. Res. B* **2012**, *668*, 88–93. [CrossRef]
28. Hiyama, F.; Noguchi, T.; Koshimizu, M.; Kishimoto, S.; Haruki, R.; Nishikido, F.; Fujimoto, Y.; Aida, T.; Takami, S.; Adschiri, T.; et al. X-ray detection properties of plastic scintillators containing surface-modified Bi_2O_3 nanoparticles. *Jpn. J. Appl. Phys.* **2018**, *57*, 052203. [CrossRef]
29. Hwang, J.; Jeon, B.; Kim, J.; Kim, H.; Cho, G. Deep learning-based spectrum-dose prediction for a plastic scintillation detector. *Radiat. Phys. Chem.* **2022**, *201*, 110444. [CrossRef]
30. Joukainen, H.; Sarén, J.; Ruotsalainen, P. Position sensitive plastic scintillator for beta particle detection. *Nucl. Instrum. Methods Phys. Res. B* **2022**, *1027*, 166253. [CrossRef]
31. Ryabeva, E.V.; Urupa, I.V.; Lupar, E.E.; Kadilin, V.V.; Skotnikova, A.V.; Kokorev, Y.A.; Ibragimov, R.F. Calibration of EJ-276 plastic scintillator for neutron–gamma pulse shape discrimination experiments. *Nucl. Instrum. Methods Phys. Res. B* **2021**, *1010*, 165495. [CrossRef]
32. Zaman, F.; Srisittipokakun, N.; Rooh, G.; Kaewkhao, J.; Ullah, I.; Rani, M.; Kim, H.J. Development of Na_2O-MO-Bi_2O_3-B_2O_3-Sm_2O_3 glasses (MO=Ba/Mg) for laser and scintillation application. *J. Non. Cryst. Solids* **2021**, *561*, 120722. [CrossRef]
33. Wantana, N.; Kaewnuam, E.; Kim, H.J.; Kang, S.C.; Ruangtaweep, Y.; Kothan, S.; Kaewkhao, J. X-ray/proton and photoluminescence behaviors of Sm^{3+} doped high-density tungsten gadolinium borate scintillating glass. *J. Alloys Compd.* **2020**, *849*, 156574. [CrossRef]
34. Tang, J.; Lin, Z.; Tu, D.; Wei, T.; Duan, R.; Zhou, S. Design and fabrication of Tb^{3+} doped Gd_2O_3-WO_3-SiO_2 scintillating glass. *J. Non-Cryst. Solids X* **2022**, *15*, 100110. [CrossRef]
35. Amelina, A.; Mikhlin, A.; Belus, S.; Bondarev, A.; Borisevich, A.; Kuznetsova, D.; Komrotov, I.; Mechinsky, V.; Kozlov, D.; Volkov, P.; et al. $(Gd,Ce)_2O_3$-Al_2O_3-SiO_2 scintillation glass. *J. Non-Cryst. Solids* **2022**, *580*, 121393. [CrossRef]

36. Wu, Y.; Chen, D.; Li, Y.; Xu, L.; Wang, S.; Wu, S. Scintillation properties of Ce^{3+}/Tb^{3+} co-doped oxyfluoride aluminosilicate glass for exploration of X-ray imaging. *J. Lumin.* **2022**, *245*, 118762. [CrossRef]
37. Kunikata, T.; Kato, T.; Shiratori, D.; Nakauchi, D.; Kawaguchi, N.; Yanagida, T. Scintillation Properties of Li-doped ZnO Translucent Ceramic. *Sens. Mater.* **2022**, *34*, 661. [CrossRef]
38. Sun, Z.; Lu, B.; Ren, G.; Chen, H. Synthesis of Green-Emitting Gd_2O_2S:Pr^{3+} Phosphor Nanoparticles and Fabrication of Translucent Gd_2O_2S:Pr^{3+} Scintillation Ceramics. *Nanomaterials* **2020**, *10*, 1639. [CrossRef]
39. Trofimov, A.A.; DeVol, T.A.; Jacobsohn, L.G. Comparative investigation of transparent polycrystalline ceramic and single crystal $Lu_3Al_5O_{12}$:Ce scintillators: Microstructural and thermoluminescence analyses. *J. Lumin.* **2021**, *238*, 118229. [CrossRef]
40. Seeley, Z.M.; Cherepy, N.J.; Payne, S.A. Homogeneity of Gd-based garnet transparent ceramic scintillators for gamma spectroscopy. *J. Cryst. Growth* **2013**, *379*, 79–83. [CrossRef]
41. Li, J.; Song, J.; Li, W.; Mei, B.; Liu, Z.; Zhang, Y. Fabrication and scintillation characterizations of high concentration Ce^{3+} doped BaF_2 transparent ceramic. *Nucl. Instrum. Methods Phys. Res. B* **2020**, *980*, 164497. [CrossRef]
42. Okazaki, K.; Onoda, D.; Nakauchi, D.; Kawano, N.; Fukushima, H.; Kato, T.; Kawaguchi, N.; Yanagida, T. Scintillation Properties of an Organic–Inorganic Lead Iodide Perovskite Single Crystal Having Quantum Well Structures. *Sens. Mater.* **2022**, *34*, 575. [CrossRef]
43. Gorbenko, V.; Zorenko, Y.; Savchyn, V.; Zorenko, T.; Pedan, A.; Shkliarskyi, V. Growth and luminescence properties of Pr^{3+}-doped single crystalline films of garnets and perovskites. *Radiat. Meas.* **2010**, *45*, 461–464. [CrossRef]
44. Jana, A.; Cho, S.; Patil, S.A.; Meena, A.; Jo, Y.; Sree, V.G.; Park, Y.; Kim, H.; Im, H.; Taylor, R.A. Perovskite: Scintillators, direct detectors, and X-ray imagers. *Mater. Today* **2022**, *55*, 110–136. [CrossRef]
45. Li, Y.; Li, Q.-L.; Li, Y.; Yang, Y.-L.; Zhang, S.-L.; Zhao, J.; Wan, J.; Zhang, Z. Water-assistant ultrahigh fluorescence enhancement in perovskite polymer-encapsulated film for flexible X-ray scintillators. *Chem. Eng. J.* **2023**, *452*, 139132. [CrossRef]
46. Dorenbos, P. The quest for high resolution γ-ray scintillators. *Opt. Mater. X* **2019**, *1*, 100021. [CrossRef]
47. Pidol, L.; Kahn-Harari, A.; Viana, B.; Virey, E.; Ferrand, B.; Dorenbos, P.; de Haas, J.T.M.; van Eijk, C.W.E. High efficiency of lutetium silicate scintillators, Ce-doped LPS, and LYSO crystals. *IEEE Trans. Nucl. Sci.* **2004**, *51*, 1084–1087. [CrossRef]
48. Feng, H.; Ding, D.; Li, H.; Lu, S.; Pan, S.; Chen, X.; Ren, G. Cerium concentration and temperature dependence of the luminescence of $Lu_2Si_2O_7$:Ce scintillator. *J. Alloys Compd.* **2011**, *509*, 3855–3858. [CrossRef]
49. Pidol, L.; Kahn-Harari, A.; Viana, B.; Basset, G.; Calvat, C.; Chambaz, B.; Ferrand, B. Czochralski growth and physical properties of cerium-doped lutetium pyrosilicate scintillators Ce^{3+}: $Lu_2Si_2O_7$. *J. Cryst. Growth* **2005**, *275*, e899–e904. [CrossRef]
50. Yan, C.; Zhao, G.; Hang, Y.; Zhang, L.; Xu, J. Comparison of cerium-doped $Lu_2Si_2O_7$ and Lu_2SiO_5 scintillators. *J. Cryst. Growth* **2005**, *281*, 411–415. [CrossRef]
51. Pidol, L.; Viana, B.; Kahn-Harari, A.; Ferrand, B.; Dorenbos, P.; Van Eijk, C.W.E. Scintillation and thermoluminescence properties of $Lu_2Si_2O_7$: Ce^{3+} crystals. *Nucl. Instrum. Methods Phys. Res. B* **2005**, *537*, 256–260. [CrossRef]
52. Pidol, L.; Guillot-Noël, O.; Kahn-Harari, A.; Viana, B.; Pelenc, D.; Gourier, D. EPR study of Ce^{3+} ions in lutetium silicate scintillators $Lu_2Si_2O_7$ and Lu_2SiO_5. *J. Phys. Chem. Solids* **2006**, *67*, 643–650. [CrossRef]
53. Kantuptim, P.; Kato, T.; Nakauchi, D.; Kawaguchi, N.; Yanagida, T. Ce concentration dependence on scintillation properties of Ce-doped yttrium pyrosilicate single crystal. *Radiat. Phys. Chem.* **2022**, *197*, 110160. [CrossRef]
54. Kantuptim, P.; Akatsuka, M.; Nakauchi, D.; Kato, T.; Kawaguchi, N.; Yanagida, T. Tm concentration dependence of scintillation characteristics on Tm-doped $Lu_2Si_2O_7$ single crystal. *J. Alloys Compd.* **2020**, *847*, 156542. [CrossRef]
55. Watanabe, K.; Yanagida, T.; Nakauchi, D.; Kawaguchi, N. Scintillation light yield of Tb:$Sr_2Gd_8(SiO_4)_6O_2$. *Jpn. J. Appl. Phys.* **2021**, *60*, 106002. [CrossRef]
56. Yanagida, T.; Kamada, K.; Fujimoto, Y.; Yagi, H.; Yanagitani, T. Comparative study of ceramic and single crystal Ce: GAGG scintillator. *Opt. Mater.* **2013**, *35*, 2480–2485. [CrossRef]
57. Yanagida, T.; Fujimoto, Y.; Ito, T.; Uchiyama, K.; Mori, K. Development of X-ray-induced afterglow characterization system. *Appl. Phys. Express* **2014**, *7*, 18–21. [CrossRef]
58. Fukushima, H.; Nakauchi, D.; Kawaguchi, N.; Yanagida, T. Photoluminescence and Scintillation Properties of Ce-doped $SrHfO_3$. *Sens. Mater.* **2019**, *31*, 1273. [CrossRef]
59. Kantuptim, P.; Akatsuka, M.; Nakauchi, D.; Kato, T.; Kawaguchi, N.; Yanagida, T. Optical and Scintillation Properties of Nd-doped $Lu_2Si_2O_7$ Single Crystals. *J. Alloys Compd.* **2020**, *860*, 158538. [CrossRef]
60. Holl, I.; Lorenz, E.; Mageras, G. A measurement of the light yield of common inorganic scintillators. *IEEE Trans. Nucl. Sci.* **1988**, *35*, 105–109. [CrossRef]
61. Wolff, N.; Klimm, D. Determination of the phase diagram Tb_2O_3–SiO_2 and crystal growth of the rare earth pyrosilicate $Tb_2Si_2O_7$ by the optical floating-zone (OFZ) technique. *J. Solid State Chem.* **2022**, *312*, 123269. [CrossRef]
62. Feng, H.; Xu, W.; Ren, G.; Yang, Q.; Xie, J.; Xu, J.; Xu, J. Optical, scintillation properties and defect study of $Gd_2Si_2O_7$:Ce single crystal grown by floating zone method. *Phys. B Condens. Matter* **2013**, *411*, 114–117. [CrossRef]
63. Kantuptim, P.; Akatsuka, M.; Nakauchi, D.; Kato, T.; Kawaguchi, N.; Yanagida, T. Scintillation properties of Pr-doped $Lu_2Si_2O_7$ single crystal. *Radiat. Meas.* **2020**, *134*, 106320. [CrossRef]
64. Kantuptim, P.; Akatsuka, M.; Kawaguchi, N.; Yanagida, T. Optical and scintillation properties of Pr-doped $Y_2Si_2O_7$ single crystal. *Jpn. J. Appl. Phys.* **2020**, *59*, SCCB17. [CrossRef]

65. Kantuptim, P.; Akatsuka, M.; Nakauchi, D.; Kato, T.; Kawaguchi, N.; Yanagida, T. Scintillation Characteristics of Pr-doped $Gd_2Si_2O_7$ Single Crystal. *Sens. Mater.* **2020**, *32*, 1357. [CrossRef]
66. Kantuptim, P.; Kato, T.; Nakauchi, D.; Kawaguchi, N.; Yanagida, T. Scintillation Properties of Pr-Doped Lanthanum Pyrosilicate Single Crystals. *Crystals* **2022**, *12*, 459. [CrossRef]
67. Kantuptim, P.; Fukushima, H.; Kimura, H.; Nakauchi, D.; Kato, T.; Koshimizu, M.; Kawaguchi, N.; Yanagida, T. VUV- and X-ray-induced Properties of $Lu_2Si_2O_7$, $Y_2Si_2O_7$, and $Gd_2Si_2O_7$ Single Crystals. *Sens. Mater.* **2021**, *33*, 2195. [CrossRef]
68. Kawano, N.; Akatsuka, M.; Kimura, H.; Okada, G.; Kawaguchi, N.; Yanagida, T. Scintillation and TSL properties of Tb-doped $NaPO_3$-$Al(PO_3)_3$ glasses. *Radiat. Meas. J.* **2018**, *117*, 52–56. [CrossRef]
69. Matsuo, T.; Kato, T.; Kimura, H.; Nakamura, F.; Nakauchi, D.; Kawaguchi, N.; Yanagida, T. Evaluation of dosimetric properties of Tb-doped Mg F_2 transparent ceramics. *Optik* **2020**, *203*, 163965. [CrossRef]
70. Nakauchi, D.; Kato, T.; Kawaguchi, N.; Yanagida, T. Characterization of Eu-doped Ba_2SiO_4, a high light yield scintillator. *Appl. Phys. Express* **2020**, *13*, 2–5. [CrossRef]
71. Nagornaya, L.; Onyshchenko, G.; Pirogov, E.; Starzhinskiy, N.; Tupitsyna, I.; Ryzhikov, V.; Galich, Y.; Vostretsov, Y.; Galkin, S.; Voronkin, E. Production of the high-quality $CdWO_4$ single crystals for application in CT and radiometric monitoring. *Nucl. Instrum. Methods Phys. Res. B* **2005**, *537*, 163–167. [CrossRef]